Lithos 318–319 (2018) 434–447

Contents lists available at ScienceDirect

Lithos

journal homepage: www.elsevier.com/locate/lithos

Transport of melt and volatiles in magmas inferred from kinetic experiments on the partial melting of granitic rocks

M. Masotta [a,*], M. Laumonier [b], C. McCammon [c]

[a] Dipartimento di Scienze della Terra, Università di Pisa, Via Santa Maria 53, 56126 Pisa, Italy
[b] Laboratoire Magmas et Volcans, Université Clermont Auvergne, CNRS, IRD, OPGC, 6 Avenue Blaise Pascal, 63178 Aubière Cedex, France
[c] Bayerisches Geoinstitut, Universität Bayreuth, 95440 Bayreuth, Germany

ARTICLE INFO

Article history:
Received 29 May 2018
Accepted 25 August 2018
Available online 30 August 2018

Keywords:
Partial melting
Granite
Pegmatites
Melt segregation
Assimilation
Trace elements

ABSTRACT

Partial melting of crustal rocks is responsible for the formation of silicic magmas and crustal differentiation. Determining the mechanisms and effects of partial melting is necessary to understand the geochemical signature of the magmas and the transport of melt and volatiles in the crust. To this end, we have experimentally reproduced the partial melting of granitic rock under three different conditions: i) partial melting in a closed system (dry and hydrous conditions); ii) partial melting in the presence of a discontinuity, represented by a channel of synthetic haplogranite and iii) assimilation of granitic rock by a hydrous trachyandesitic melt. Experiments were performed at temperatures between 750 and 1000 °C and pressures between 300 and 500 MPa, with durations ranging from 24 to 240 h. Partial melting initiates at temperatures higher than 750 °C as a result of both dehydration melting of hydrous minerals and melting at grain boundaries. The interplay between the two mechanisms determines the complex evolution of melt composition at the various degrees of partial melting. Core-to-rim compositional profiles of residual feldspars in contact with the melt attest to a rapid mineral-melt re-equilibration (240 h). When a melt channel intersects the granite, the melt produced at the grain boundaries is rapidly segregated within the channel and mineral-melt exchange reactions are inhibited. In turn, the melt in the channel is enriched in H_2O and incompatible trace elements. When in contact with a hydrous, partially molten trachyandesite, complete dissolution of the granite occurs at 900 °C, assisted by the migration of H_2O from the crystallizing trachyandesitic melt. The melting-assimilation process results in a system characterized by a crystalline trachyandesite enclosing a hybrid trachytic melt, produced by the chemical mixing of the granitic melt with the melt segregated from the crystalline trachyandesite.
Our experimental results indicate that partial melting could be extremely common in granitic bodies and yield no traces in the residual rock after segregation of the interstitial melt. In contrast, core-to-rim profiles of feldspars may preserve a record of the interaction between residual minerals and the extracted melt. Fast segregation of melts enriched in volatiles and incompatible trace elements, produced by breakdown of hydrous minerals, may represent a possible mechanism for generation of pegmatites.

1. Introduction

Partial melting is responsible for the production of large volumes of granitic melt in the Earth's crust (Kriegsman, 2001). Melting of crustal rocks typically occurs as a result of the intrusion of hot magmas, in amounts related to the temperature and mass of the intruding magma (Al-Rawi and Carmichael, 1967; Holness et al., 2005; Holness and Watt, 2002; Kaczor, 1988; Philpotts and Asher, 1993). The newly-formed melts can either concentrate into felsic domains within the host rock (*i.e.* migmatites) or segregate into dykes and apophyses, sometimes inducing further melting (Hersum et al., 2007). These two alternatives mostly depend on the mechanical state of the host rocks, as well as on the amount and physical conditions of the melt produced. In turn, the amount of melting determines the enrichment in volatile and incompatible trace elements, pointing to partial melting of granitic rocks as one of the possible mechanisms for the formation of pegmatites (London and Morgan VI, 2012).

The role of volatiles is of primary importance in controlling both the kinetics and degree of partial melting. When H_2O is present in the system, larger amounts of melts can be produced by partial melting of granitic rocks, since melting temperatures of quartz-feldspatic mineral assemblages are significantly lower (Clemens and Droop, 1998; Luth, 1969; Stevens and Clemens, 1993; Tuttle and Bowen, 1958). However, due to the low amount of H_2O that can be stored within mineral grain boundaries, a contribution of external water is generally required to

* Corresponding author.
E-mail address: matteo.masotta@unipi.it (M. Masotta).

https://doi.org/10.1016/j.lithos.2018.08.032
0024-4937/

increase the amount of partial melting (Gaeta et al., 2018; Weinberg and Hasalová, 2015). In contrast to hydrous (*i.e.* volatile-assisted) partial melting, anhydrous partial melting (*i.e.*, no external volatiles involved) occurs at temperatures higher than the solidus of dry assemblages and involves the breakdown of hydrous minerals such as micas and amphiboles (Fyfe, 1970; Thompson, 1982). Only in some cases, when the H_2O available from hydrous minerals is significant, the amount of melt may far exceed the amount of melt produced by hydrous partial melting, reaching values up to 30 vol% (Clemens, 1984; Clemens and Vielzeuf, 1987).

The physical conditions under which partial melting of igneous rocks occurs have been constrained by many experimental studies (Acosta-Vigil et al., 2006; Attrill and Gibb, 2003a, 2003b; Brearley and Rubie, 1990; Le Breton and Thompson, 1988; Masotta et al., 2018; Patiño-Douce and Beard, 1995; Qian and Hermann, 2013; Scaillet et al., 1995; Vielzeuf and Holloway, 1988; Wolf and Wyllie, 1995). Much interest has been focussed on the granitic system on the basis of simplicity (a haplogranite can be described by the three pure components Ab, Or, Qz) and because it represents, to a first approximation, the composition of the Earth's upper crust. Following the first work on the haplogranitic system by Tuttle and Bowen (1958), further experimental studies investigated the effects produced by adding components such as CaO, FeO and MgO, in order to account for the presence of plagioclase and mafic minerals in natural rocks (Johannes and Holtz, 1996 and references therein). On the other hand, the main inconvenience of using granitic systems for experimental studies is the slow approach to thermodynamic equilibrium, which would require very long experimental times. For this reason, only few experimental studies have been carried out on natural granitic systems. Among these, Acosta-Vigil et al. (2006) investigated the textural and chemical relationships between partial melt and residual phases, whereas Attrill and Gibb (2003a, 2003b) performed partial melting and recrystallization experiments to investigate the capability of granitic rocks for radioactive waste disposal. All of these studies highlighted the paramount importance of the volatile phase (H_2O) in decreasing the temperature at which partial melting initiates, facilitating the melting reaction over relatively short time scales.

In this paper, we investigate experimentally the conditions at which partial melting in a natural granitic system occurs using three different experimental setups: i) simple partial melting of a granitic cylinder under both anhydrous and hydrous conditions, ii) melting in the presence of a solid-liquid interface (constituted by a melt channel) and iii) melting induced by contact with a hydrous intermediate magma composition. The goal of these different experimental setups is not to reproduce partial melting at thermodynamic equilibrium, but rather to provide the possibility to determine spatial and compositional relationships between the source rock and its partial melt, the efficiency of melt segregation upon melting at grain boundaries and the mobility of incompatible trace elements in crustal granitic rocks undergoing partial melting.

2. Methods

2.1. Geological setting of the starting material

A fine-textured pink metagranite from Gennargentu Igneous Complex (Sardinia, Italy) was selected as starting material for the experiments because of the small (<500 μm) and regular grain size and the homogeneous composition of minerals (Fig. 1a). The metagranite (sample GG24gf from Gaeta et al., 2013) was collected at the contact between a peraluminous granite (310 ± 6 Ma) and a quartz-diorite (306 ± 26 Ma; Gaeta et al., 2018). The intrusion of the quartz-diorite in the peraluminous granite produced a 20 m thick metamorphic aureole, consisting of pink and red metagranites, and abundant veins and lenses of porphyry that homogeneously cut the contact region between the two intrusive bodies. The mineral assemblage of the granite is

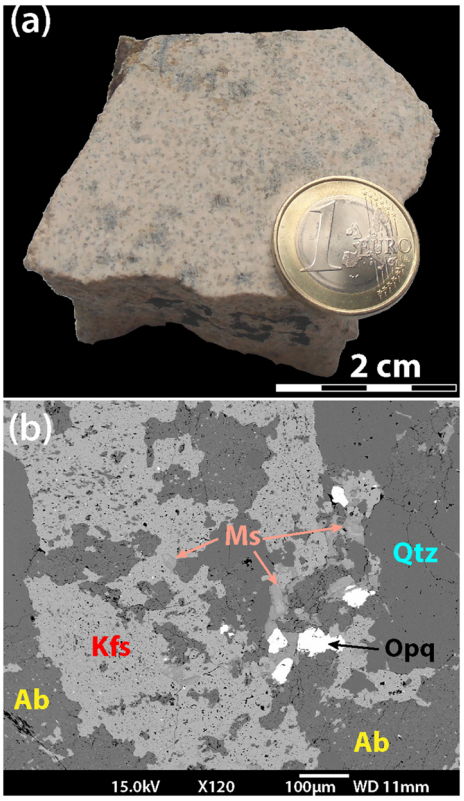

Fig. 1. (a) Photograph of the granite sample used for experiments and (b) back scattered electron (BSE) image of the sample. Abbreviations: Qtz, quartz; Kfs, K-feldspar; Ms., muscovite; Ab, albite; Opq, Opaque mineral.

constituted by quartz, albite ($An_{3-6}Ab_{93-97}Or_{0-2}$), K-feldspar ($An_{0-2}Ab_{1-5}Or_{95-98}$), muscovite, and traces of tourmaline, biotite and opaque minerals (Fig. 1b). The contacts between K-feldspar and albite are irregular, whereas those with quartz are usually sharp and faceted. This feature, as well as the homogeneous chemical composition of minerals, was preserved from the texture of the protolith (Gaeta et al., 2013). The bulk composition of the pink metagranite (hereafter referred as granite), as well as the composition of mineral phases are reported in the electronic appendix (Tables EA1 and EA2).

2.2. Sample preparation and experimental methods

Experiments were performed in piston cylinder presses at temperatures between 750 and 1000 °C and pressures between 300 and 500 MPa, with durations ranging from 24 to 240 h. Cylindrical-shaped platinum capsules (3.5 mm OD, 3.1 mm ID) were filled with different combinations of starting materials, depending on the experimental setup (Fig. 2): setup 1 was used for both anhydrous partial melting (APM) and hydrous partial melting (HPM) experiments, setup 2 for segregation partial melting (SPM) experiments and setup 3 for assimilation melting experiments (ASM). Sample capsules for APM and HPM experiments (setup 1) were filled by 3-mm tall cylindrical granitic cores. About 5 wt% of deionized water was added to HPM capsules only. For SPM experiments (setup 2), a 1-mm diameter hole was drilled along the axis of the granitic cores and filled with a powder of synthetic haplogranite. For ASM experiments (setup 3), capsules were filled with a core of granite that was centred in the capsule and surrounded by powder of a synthetic hydrous trachyandesite (H_2O = 5 wt%). The granitic cores used as starting materials were directly drilled from the bulk granite sample and used for experiments after checking under an optical microscope for homogeneous grain size and mineralogy. The trachyandesitic and haplogranitic glasses are the same ones used in Masotta and Keppler (2015). These were synthesized by melting a

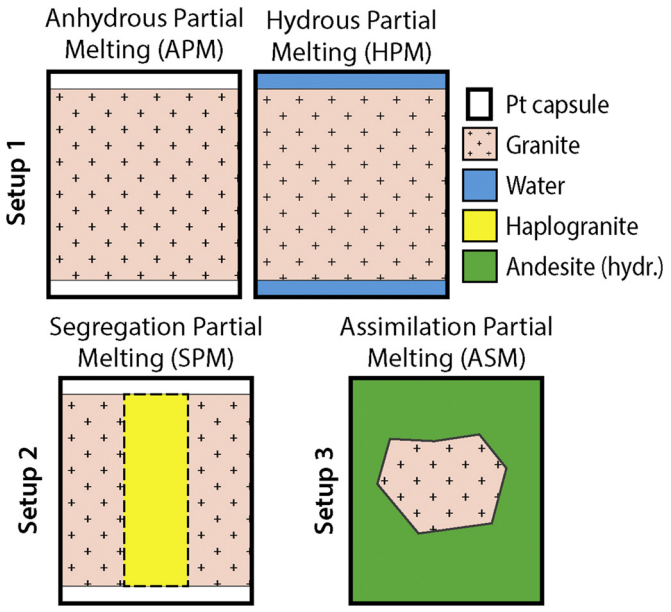

Fig. 2. Schematic representation of the three experimental setups adopted.

mixture of analytical grade oxides and carbonates in a platinum crucible that was placed in a chamber furnace at 1600 °C for 2 h, resulting in clear, bubble-free glasses. Hydrous glass was prepared by melting the synthetic trachyandesite plus 6 wt% of deionized water in a platinum capsule at 1100 °C and 200 MPa in a cold sealed TZM apparatus.

The same experimental procedure ("hot piston in") was followed for all the experiments: the assembly is cold pressurized to a pressure 10% lower than the desired experimental pressure, temperature is then increased at a constant rate (100 °C/min) before the pressure is increased to the target pressure. At the end of the experiment, a nearly isobaric quench is obtained by shutting off the power supply and compensating the pressure drop upon cooling. Temperature during the experiments was constantly monitored using factory calibrated S-type thermocouple, with a maximum error of ±5 °C. Most experiments were performed in an end-loaded piston cylinder press at the *Bayerisches Geoinstitut* (BGI, University of Bayreuth, Germany), using standard 19 mm crushable alumina-borosilicate glass-talc assemblies to reach a target pressure of 500 MPa. Experiments carried out at 300 MPa were performed in a non-end-loaded piston cylinder (QUICKpress by Depths of the Earth Co.) installed at the HP-HT Laboratory of Experimental Volcanology and Geophysics of the *Istituto Nazionale di Geofisica e Vulcanologia* (INGV, Rome, Italy). These latter experiments were conducted using a 19–25 mm crushable MgO-borosilicate glass-NaCl assembly specific for experiments at pressures below 500 MPa. The assembly materials yield an intrinsic oxygen fugacity close to NNO + 2 (Masotta et al., 2012a).

All capsules from experimental runs were cut in half, mounted in epoxy disks and polished to expose the surface of the granite fragments or the haplogranite-filled cavity. A summary of experimental conditions is reported in Table 1.

2.3. Analytical methods

Images were collected both at the INGV using the backscattered electron (BSE) mode of a field emission gun-scanning electron microscope (FE-SEM) JEOL 6500F equipped with an energy-dispersive spectrometer (EDS) detector. Chemical analyses on glasses and minerals were obtained with a JEOL JXA-8200 electron microprobe (EMP) installed at BGI, using a 10-μm defocused beam, accelerating voltage of 15 kV and current of 15 nA. The following standards were used: albite (Si, Na), rutile (Ti), spinel (Al), andradite (Ca, Fe), forsterite (Mg), orthoclase (K) and barium sulphate (S). Acquisition time was set to 20 s for peak and 10 s for background. Alkalis were analysed before other elements to minimize their loss during analysis. Trace elements were analysed using a LA-ICP-MS system installed at BGI, composed of a

Table 1
List of experiments.

Experiment	T (°C)	P (MPa)	t (h)	%PM[a]	Residual minerals	New minerals
Setup 1 - Anhydrous Partial Melting (APM)						
^{24h}APM-750	750	500	24	0%	Qtz + Kfs + Ab+Ms. + Opq	–
^{120h}APM-750	750	500	120	0%	Qtz + Kfs + Ab+Ms. + Opq	Crn
^{24h}APM-800$_{300}$	800	300	24	<5%	Qtz + Kfs + Ab+Ms. + Opq	–
^{24h}APM-800	800	500	24	<5%	Qtz + Kfs + Ab+Ms. + Opq	–
^{120h}APM-800	800	500	120	<5%	Qtz + Kfs + Ab+Ms. + Opq	Crn + Kfs + Bt
^{24h}APM-850$_{300}$	850	300	24	5–10%	Qtz + Kfs + Ab+Opq	Crn + Kfs + Bt
^{24h}APM-850	850	500	24	10–15%	Qtz + Kfs + Ab+Opq	Crn + Kfs + Bt
^{120h}APM-850	850	500	120	10–15%	Qtz + Kfs + Ab+Opq	Crn + Kfs + Bt
^{240h}APM-850	850	500	240	10–15%	Qtz + Kfs + Ab+Opq	Crn + Kfs + Bt
^{24h}APM-900$_{300}$	900	300	24	15–20%	Qtz + Kfs + Ab+Opq	Crn + Kfs + Bt
^{24h}APM-900	900	500	24	15–20%	Qtz + Kfs + Ab+Opq	Crn + Kfs + Bt
Setup 1 - Hydrous Partial Melting (HPM)						
^{24h}HPM-800	800	500	24	20–25%	Qtz + Kfs + Ab+Opq	Crn + Kfs + Bt
^{72h}HPM-800	800	500	72	25–30%	Qtz + Kfs + Ab+Opq	Crn + Kfs + Bt
^{24h}HPM-850	850	500	24	30–40%	Qtz + Kfs + Opq	Kfs
^{24h}HPM-900	900	500	24	70%	Qtz + Opq	–
Setup 2 - Segregation Partial Melting (SPM)						
^{72h}SPM-850	850	500	72	–	Qtz + Kfs + Ab+Opq	–
^{24h}SPM-900	900	500	24	–	Qtz + Kfs + Ab+Opq	Kfs
^{240h}SPM-900	900	500	240	–	Qtz + Kfs + Ab+Opq	Kfs
^{24h}SPM-950	950	500	24	–	Qtz + Kfs + Ab+Opq	Kfs
Setup 3 - Assimilation Partial Melting (ASM)						
^{24h}ASM-900	900	500	24	100%	–	Cpx + Fsp
^{24h}ASM-950	950	500	24	100%	–	Cpx + Fsp
^{240h}ASM-950	950	500	240	100%	–	Cpx + Fsp
^{24h}ASM-1000	1000	500	24	100%	–	Cpx + Fsp

[a] Degree of partial melting indicated as fraction of melt produced (vol%).

193 nm Excimer Laser (Lambda Physik, Germany), special energy homogenization optics (Microlas, Germany), and an Elan 6100 quadrupole mass spectrometer (Perkin Elmer, Canada). Technical information on the instrument and details of the analytical technique are given in Audédat and Pettke (2006) and Pettke et al. (2004).

The whole rock trace element content of the granite and haplogranite glass was determined by Inductively Coupled Plasma - Mass Spectrometry (ICP-MS) using a Perkin-Elmer NexION® 300× spectrometer at the Department of Earth Sciences at the University of Pisa (Italy). The geochemical reference samples WS-E (basalt) and RGM-1 (rhyolite) were dissolved and analysed along with the samples to check the accuracy of the results. About 50–100 mg of each powder were dissolved in a mixture of HF and HNO_3 on a hot plate at ~120 °C inside screw-top perfluoroalkoxy (PFA) vessels. At the end of the dissolution, the sample solutions were diluted to 50 mL in polypropylene vials. In each step of sample preparation, Mill-Q® purified water (18.2 M cm) and ultrapure HF and HNO_3 were used. The sample solutions were introduced into the plasma after online mixing with a solution containing 20 ng/mL each of Rh, Re and Bi as internal standards. The elements Li, Be, Ga, Rb, Sr, Y, Zr, Nb, Mo, Cs, Ba, REE, Hf, Ta, Pb, Th and U were determined in "standard mode", whereas the elements Sc, V, Cr, Co and Ni were determined in "kinetic energy discrimination mode, KED" using a He flow of 3.7 mL/min. Analyses were done using an external calibration performed with a solution of the BEN (alkaline basalt) geochemical reference sample. The analytical precision is between 3 and 5% RSD for elements with concentrations >5 μg/g and between 5 and 10% RSD for elements with concentrations < 5 μg/g.

3. Results

3.1. Textural features of experimental products

Anhydrous Partial Melting (APM) experiments performed at 750 °C with run durations of 24 and 240 h did not produce partial melting of the granite. However, in contrast to the 24 h experiment that preserved the original texture and mineral assemblage, the 240 h experiment displayed signs of incipient breakdown of muscovite with formation of corundum and K-feldspar within the reacting muscovite crystals (Fig. 3a–b). At 800 °C partial melting occurred along some of the albite-quartz and K-feldspar-quartz boundaries, forming a 5 μm thick layer of melt in the mantle of reacting muscovite crystals. In the 120 h experiment, corundum, K-feldspar and biotite crystallized within melt pockets produced by incomplete breakdown of muscovite (Fig. 3c). Crystal habits range from acicular for corundum to tabular for K-feldspar and biotite, and show a characteristic orientation parallel to the (001) cleavage of muscovite (Fig. 3c). The amount of melt produced at this temperature is lower than 5 vol%, independent of pressure and run duration. Complete breakdown of muscovite is observed at 850 °C, where the amount of melt increased significantly (up to 15 vol%), forming an interconnected network along mineral boundaries (albite-quartz, K-feldspar-quartz and some albite-K-feldspar boundaries). The melt layer has a nearly constant thickness of 20 μm. Tabular crystals of K-feldspar and biotite formed within the melt pockets left after the dissolution of muscovite, along with acicular-prismatic crystals of corundum (Fig. 3d). Euhedral facets of large K-feldspars in contact with the melt indicate that this mineral formed by epitaxial growth on pre-existing crystals. All these features are more pronounced in the 240 h experiment at 850 °C, and in the 24 h experiment at 900 °C, where sieve-textures composed by a mixture of relic and new feldspars are produced (Fig. 3e–f).

Hydrous Partial Melting (HPM) experiments showed a significantly higher degree of partial melting compared to APM experiments performed at the same temperature (Table 1). In experiments performed at 800 °C with run durations of 24 and 72 h, the melt layer formed at the grain boundaries has an average thickness of 100 μm and constitutes >20 vol%, which is about 4–5 times the fraction determined under the same conditions but for dry samples (APM). The breakdown of muscovite is complete and produced pockets of melts from which corundum, K-feldspar and biotite crystallized in acicular to tabular shapes, most likely aligned parallel to the (001) cleavage plane of the dissolved muscovite. In contrast, the dissolution of albite and K-feldspar crystals (mostly along cleavage planes), followed by epitaxial growth at the crystal rims, produced a sieve-texture representing a mixture of relic and new feldspars (Fig. 3g). In the experiment at 850 °C, the thickness of the melt layer at the K-feldspar-quartz grain boundaries is >100 μm and large pockets of melt formed among crystal aggregates (the amount of melt is 30–40 vol%). Where preserved, relic crystals of K-feldspar display sieve-textures that indicate a pervasive dissolution along cleavage planes followed by epitaxial recrystallization. The melt fraction increases with temperature, reaching about 70 vol% at 900 °C. In this experiment, all minerals are completely dissolved with the exception of quartz, occurring in rounded grains surrounded by bubbles (Fig. 3h). Run duration appears to have no effect on hydrous partial melting.

Segregation Partial Melting (SPM) experiments were performed in the temperature range 850–950 °C in order to produce different degrees of partial melting in the granite (10 to 25 vol% melt), as deduced from APM experiments (Table 1). The amount of melt observed at the grain boundaries, however, was much smaller than that observed in APM experiments, with an average thickness of melt network veins of <10 μm (Fig. 4). Notably, melt interconnectivity decreases from the centre to the outer parts of the capsule (which is far from the haplogranite channel). In the experiment performed at 850 °C for 72 h, the contact between the haplogranitic melt and the granite core is straight and consists of a thin (<10 μm) layer of K-feldspar crystallized at the edge of the residual feldspars (Fig. 4a). Such a K-feldspar layer is absent from the experiment conducted at 900 °C for 24 h, although the contact between the haplogranitic melt and the granite core is equally straight (Fig. 4b). At the same temperature but longer run duration (240 h), the contact becomes irregular and the haplogranitic melt infiltrates within mineral grains adjacent to the haplogranite melt channel, disassembling the granite (Fig. 4c). The same texture is observed at 950 °C. K-feldspars embedded in this pervasive melt show evidence of dissolution and recrystallization at their rims. In all the experiments, small patches of melt, corundum, K-feldspar and biotite formed inside the granite core where muscovite underwent breakdown. Bubbles are observed in these patches of melt, in melt veins at the grain boundaries and in the central haplogranite melt channel, adjacent to the melt veins (Fig. 4b).

Assimilation Melting (ASM) experiments were performed at temperatures of 900 to 1000 °C in order to prevent extensive crystallization of the trachyandesite (as deduced from experimental results from Masotta and Keppler, 2015). The higher temperature and the presence of water diffusing from the trachyandesite favoured the complete dissolution of the granite rock fragments. In all the experiments, the dissolution of granite produced a large batch of melt in the middle of the capsule, with small isolated patches (<400 μm) of clinopyroxene crystals (size of <20 μm), and bubbles of variable size from 50 μm to over 500 μm (Fig. 5). Conversely, in the trachyandesite portions, small (<10 μm) crystals of clinopyroxene, Fe-Ti-oxides and plagioclase crystallized in variable amounts, depending on experimental temperature (the crystal fraction increases from 30 vol% at 1000 °C to about 60 vol% at 900 °C). Notably, in all the experiments, a 50 μm thick layer of feldspar (Fig. 5b) and a 200 μm thicker layer of small (<2 μm) bubbles formed at the interface between the molten granite and the hydrous trachyandesite (Fig. 5d). Bubbles were also observed in the hydrous trachyandesite portions in amounts increasing with increasing crystal content. In this set of experiments, the duration seems to have no effect on the variability of the features observed or on the degree of mingling between the two domains.

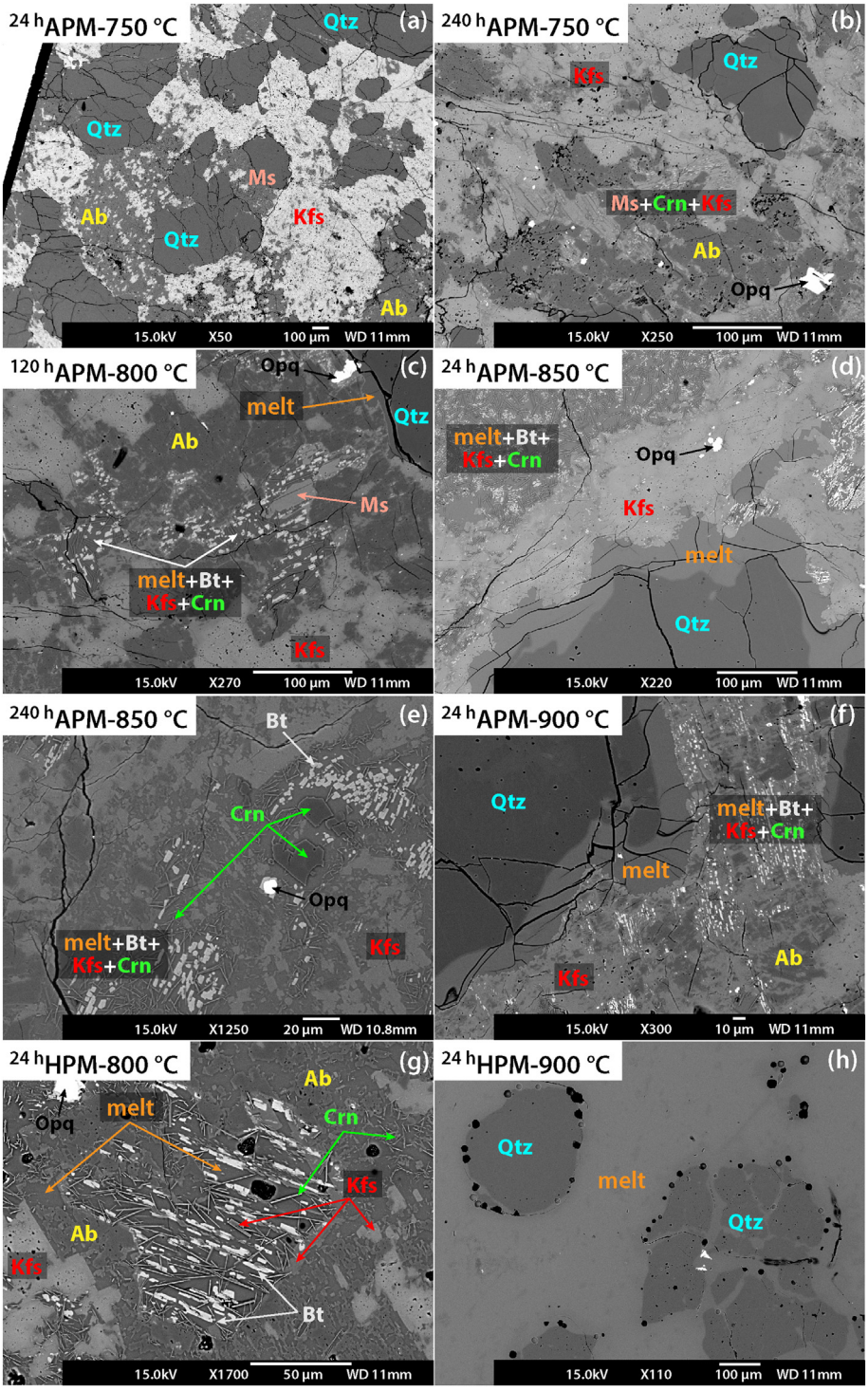

Fig. 3. BSE microphotographs of anhydrous (a-f) and hydrous (g–h) partial melting experiments. Partial melting initiates at 800 °C and increases with temperature. Melt is located at the grain boundaries and in pockets left after muscovite dissolution (d–e). Abbreviations: Qtz, quartz; Kfs, K-feldspar; Ms., muscovite; Bt, Biotite; Ab, albite; Crn, corundum; Opq, Opaque mineral.

3.2. Chemical features of experimental products

3.2.1. Glass

At low degrees of partial melting (melt up to 20 vol%), the melt composition of both APM and HPM experiments ranges in SiO_2 from 69 to 79 wt% and in total alkali ($Na_2O + K_2O$) from 8 to 11 wt% (Fig. 6a; Table EA1). Spot analyses plot along trends defined by the composition of the minerals that contribute to partial melting, which are muscovite, quartz and alkali feldspars. The melt composition is overall similar to that of the bulk granite in terms of SiO_2 and total alkali, although FeO and CaO concentrations slightly differ, and the Na_2O/K_2O ratio is lower in the experimental products. At increasing degree of partial melting (with melt ranging from 20 to 70 vol%), melt composition evolves towards less felsic composition, with SiO_2 decreasing from 77 to 67 wt% and total alkali increasing from 8 to 13 wt%. The manifest linear trend defined by HPM experiments appears directly correlated with the degree of melting, with the melt produced at 900 °C showing the lowest SiO_2 content, as a result of the melting of all the minerals except quartz

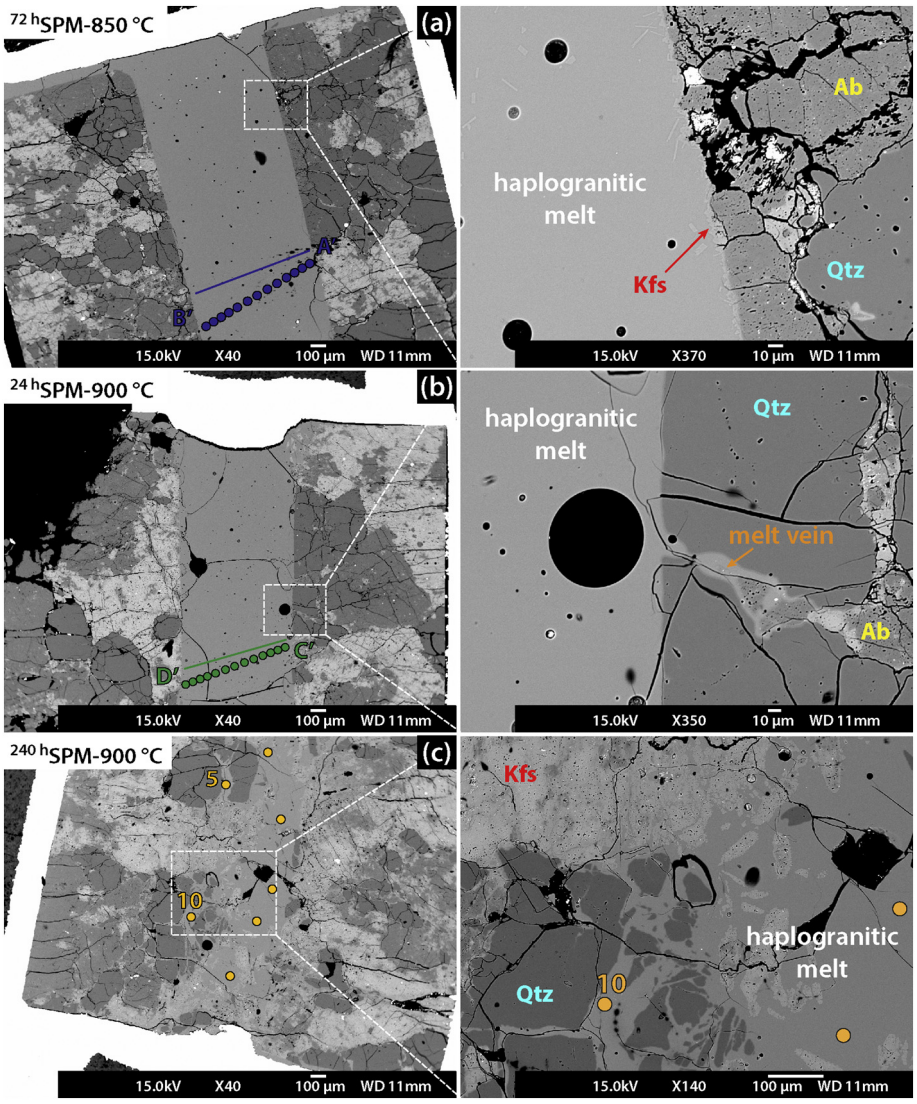

Fig. 4. BSE microphotographs of segregation partial melting (SPM) experiments showing the transverses performed during microprobe (solid line) and laser ablation (filled circles) analyses. The insets indicate the location of the images on the right sides. Abbreviations: Qtz, quartz; Kfs, K-feldspar; Ab, albite. The melt layer on top of the granite in panel (a) is the haplogranite powder that remained in the capsule after filling the channel during sample preparation.

(Fig. 3h). The amount of H_2O in the melt from APM experiments (estimated by difference from the EMP total; Devine et al., 1995) is inversely proportional to the amount of melt produced, increasing from 2 wt% in the experiment performed at 900 °C and 300 MPa (melt = 20 vol%) to 8 wt% in the experiment performed at 800 °C and 500 MPa (melt < 5 vol%) (Table EA1). In a similar fashion, the Alumina Saturation Index (ASI), calculated as the molar ratio $Al_2O_3/(CaO + Na_2O + K_2O)$, decreases from about 1.3 to about 1.1 with increasing degree of partial melting (0–20%) and shows a positive correlation with the water content in the melt (Fig. 6b). At degrees of partial melting higher than 20%, as in the case of the HPM experiments, the ASI values further decrease from about 1.1 to about 1.0 (Table EA1).

In SPM experiments, the SiO_2 content of the haplogranite melt channel increases from 76 wt% at 850 °C to almost 80 wt% at 950 °C, whereas the total alkali shows a negative correlation with temperature and SiO_2 (Fig. 6c). The melt analysed at the grain boundaries yields lower SiO_2 and slightly higher total alkali content (Table EA1). The negative correlation between the ASI value and the Na_2O (Fig. 6d) results from an increasing contamination of the haplogranite by the melt produced by partial melting of the granite at increasing experimental temperature. Compositional transverses across the central melt channel display rather smooth and homogeneous profiles, with weak variations of SiO_2 and Na_2O towards the contacts where mineral-melt cation exchange between the feldspars and the haplogranitic melt occurred (Fig. 7a). Trace elements were also analysed across the central haplogranite channel following the same transverses used for the analysis of major elements (Fig. 4a–b) or, where the original shape of the melt channel was not preserved (*i.e.* 240 h experiment at 900 °C), trace element analyses were performed randomly in the haplogranitic melt (Fig. 4c). The haplogranitic melt is always enriched in incompatible trace elements released during the partial melting of the granite and eventually concentrated in the melt channel (Fig. 7b). The enrichment varies with the progress of partial melting, with some elements (Li, B, Sr, Y, La, Ce, Nd, and Dy) being more enriched at low degrees of partial melting (*i.e.* 24 h experiments at 850 and 900 °C) and other elements (Cs, W, Pb, U, Th) becoming enriched at higher degrees (*i.e.* 240 h experiment at 900 °C; Table EA3). It is worth noting that the elements enriched at lower degrees of partial melting (*i.e.* Li and Sr) display an opposite concentration profile compared to those enriched at higher degrees of partial melting (*i.e.* Cs and Pb), yielding the maximum concentration in the centre and at the border of the melt channel, respectively (Fig. 7b).

Compositional transverses for major elements were carried out along the axes of the molten area of ASM experiments (some

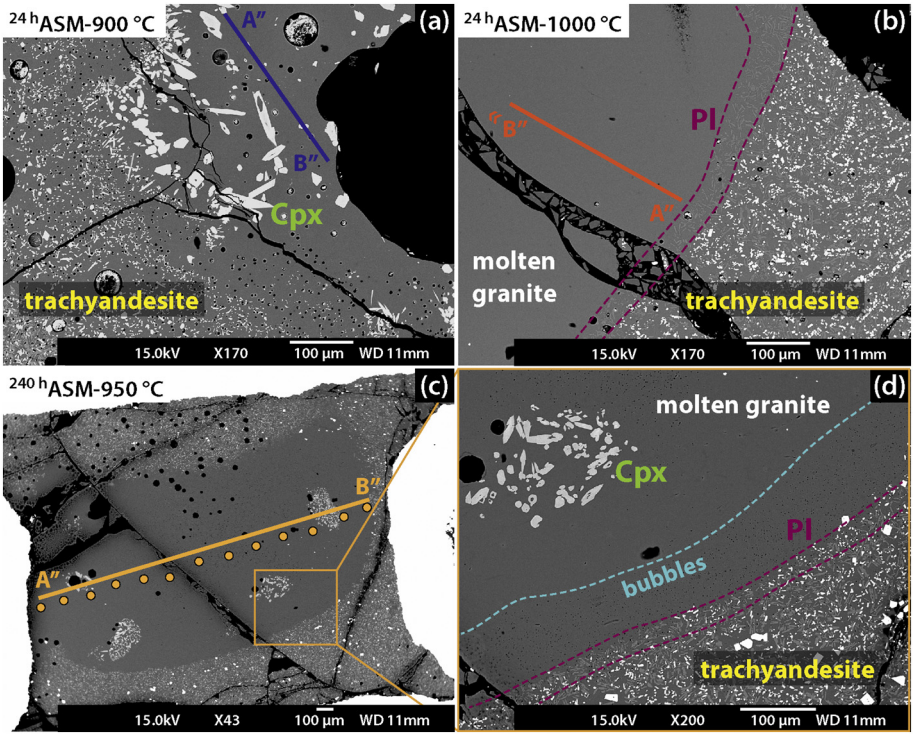

Fig. 5. BSE microphotographs of assimilation partial melting (ASM) experiments showing the transverses performed during microprobe (solid line) and laser ablation (filled circles) analyses. The orange inset in (c) indicates the location of the image on the right side. Abbreviations: Cpx, clinopyroxene; Pl, plagioclase.

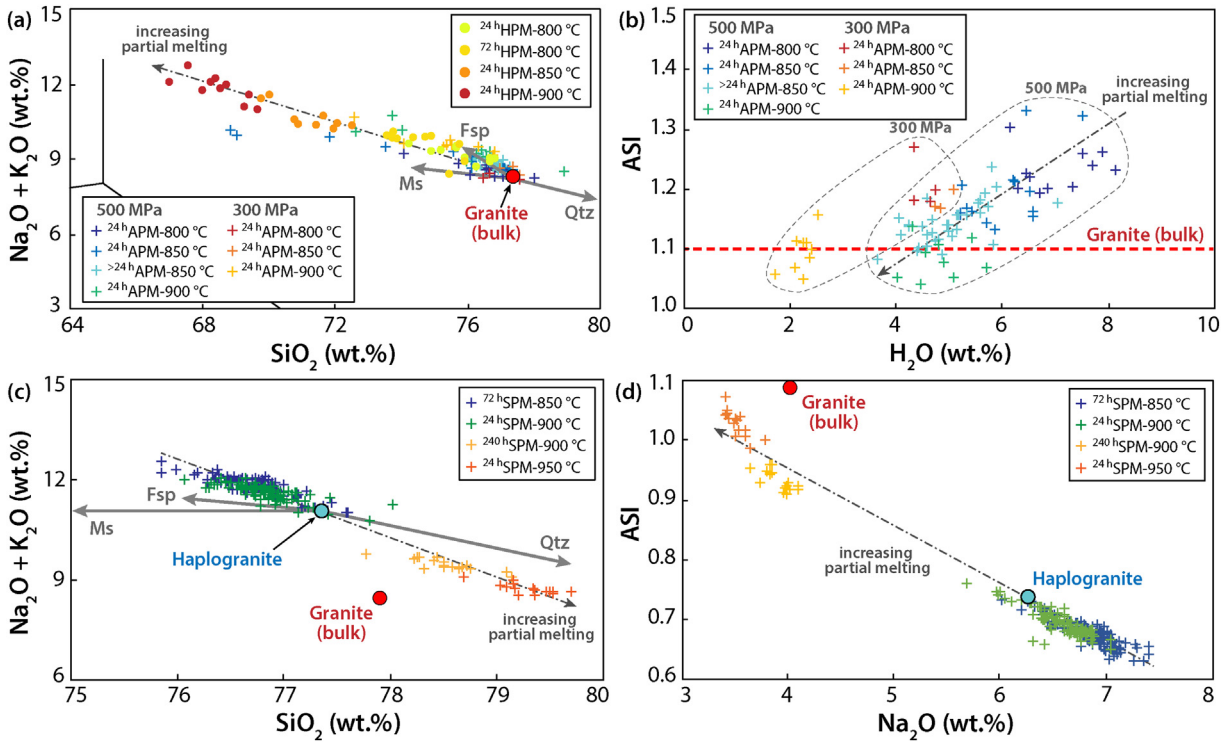

Fig. 6. (a) Total alkali *vs.* silica diagram reporting the composition of melt formed in APM and HPM experiments. Grey arrows indicate the change of melt composition resulting from addition of 10 wt% of a mineral (Ms: muscovite, Fsp: feldspars, Qtz: quartz) to the bulk composition of the granite. The alignment of points along the two left arrows indicates the prevailing melting of muscovite and feldspars. All the data that plot to the far left to the bulk granite composition represent analyses performed on melt pockets left after muscovite dissolution. (b) Alumina Saturation Index (ASI) of melt formed in APM and HPM experiments plotted against water content measured "by difference". The bulk ASI of the granite is reported for comparison (red dashed line). (c) Total alkali *vs.* silica diagram reporting the composition of the melt in the channels of SPM experiments. Grey arrows indicate the change of melt composition resulting from addition of 10 wt% of a mineral to the bulk composition of the haplogranite. (d) ASI plotted against Na_2O (wt%) in the melt. The bulk compositions of the granite and haplogranite are shown for comparison.

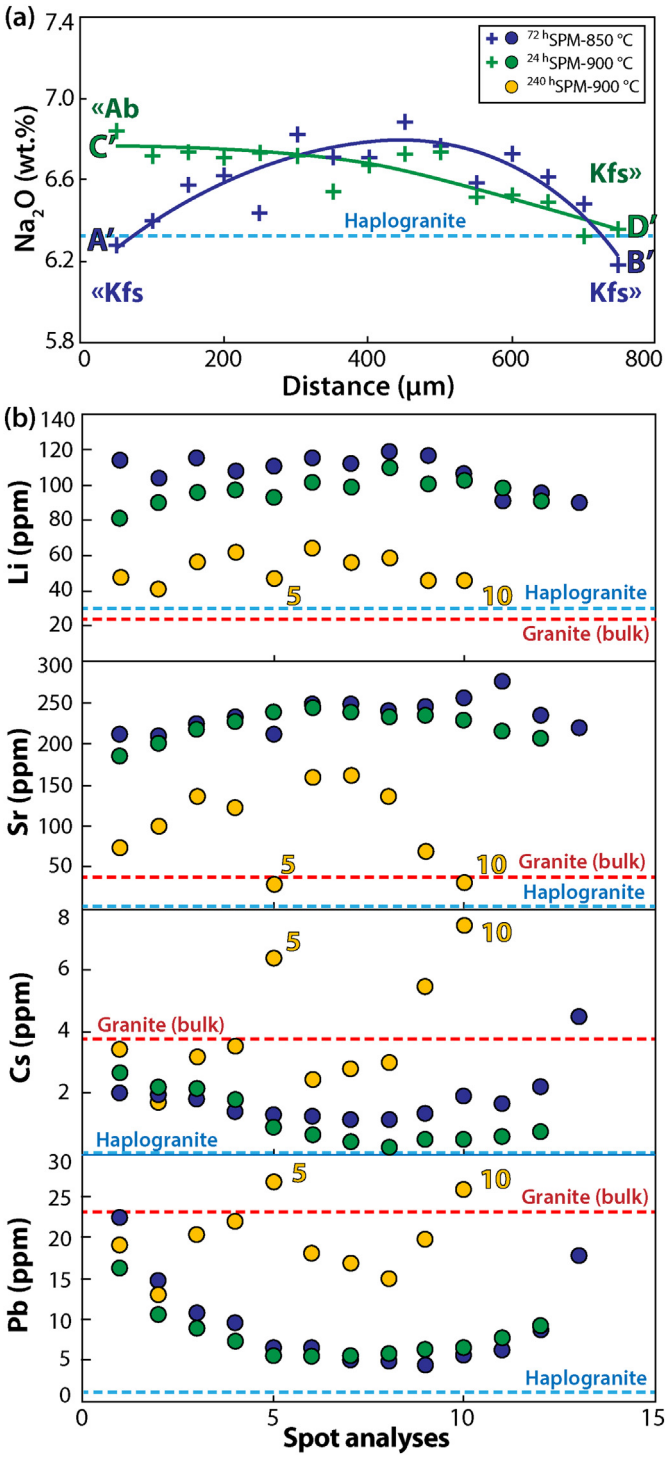

Fig. 7. (a) Na_2O (wt%) and (b) selected trace element (Li, Sr, Cs, Pb) profiles measured along the A'–B' and C'–D' lines in the central haplogranitic melt channel of SPM experiments (see location in Fig. 4). Solid lines are the visual interpolation of the data. Dashed lines indicate the bulk composition of the granite (red) and haplogranite (light blue).

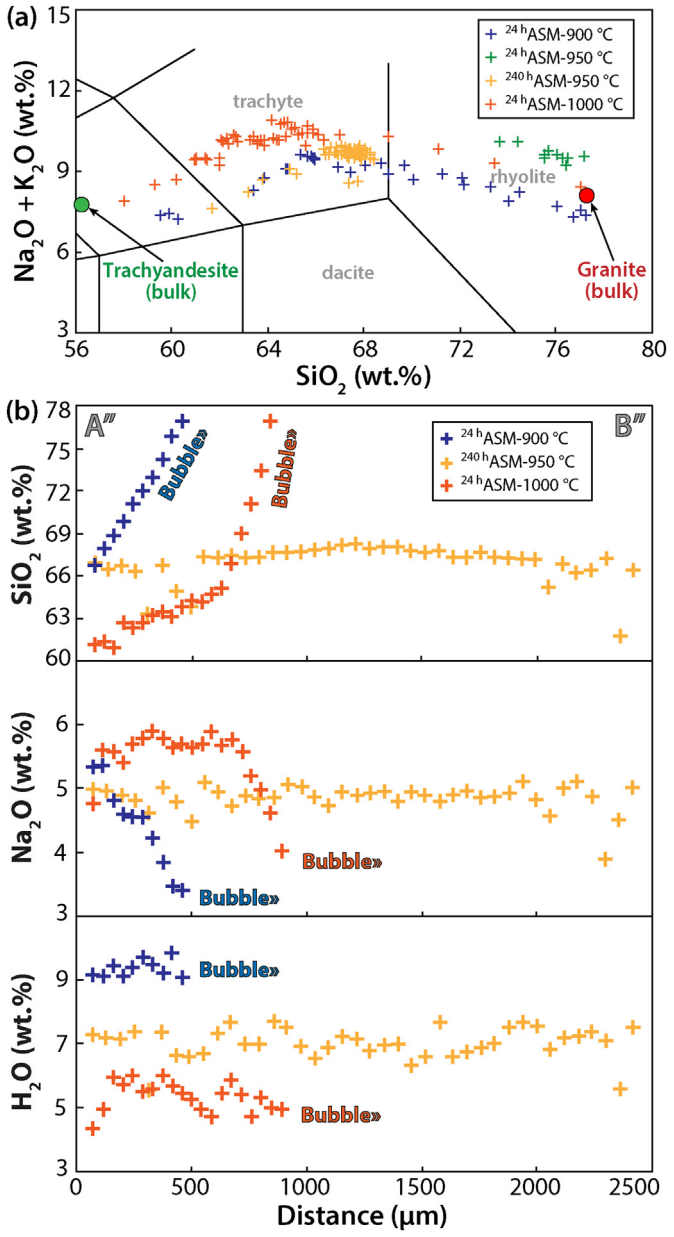

Fig. 8. (a) Total alkali *vs.* silica diagram reporting the composition of melt in ASM experiments. The bulk compositions of the granite and trachyandesite are shown for comparison. (b) Selected elements (Na_2O, SiO_2 and H_2O) profiles measured along the A ″–B″ lines in granitic melt (see location in Fig. 5).

transverses were interrupted due to the presence of a large bubble in the middle of the molten area). These transverses are not apparently affected by the initial heterogeneity of the granite and display rather linear compositional gradients with the highest SiO_2 concentration in the middle of the molten area (Fig. 8). The 240 h experiment at 950 °C displays a roughly homogeneous trachytic composition, intermediate between the bulk compositions of the trachyandesite and the granite. In contrast, the 24 h experiments show mixing trends with melt composition departing from the two end-members (Fig. 8a). Trace elements were analysed along the complete melt transect of the 240 h experiment and yielded values comparable to those of the bulk granite (Table EA3).

3.2.2. Minerals

Feldspars in APM experiments exhibit chemical compositions that diverge from those of the feldspars analysed in the starting granite with increasing degree of partial melting (Fig. 9a–b). As a result of the reaction with the melt formed during partial melting, albite becomes more potassic with a composition varying from the initial Or_{0-2} to Or_{14}, whereas K-feldspar becomes more sodic with a composition varying from the initial Ab_1 to Ab_{34}. Newly formed feldspars display a ternary composition ($An_{3-4}Ab_{62-67}Or_{31-35}$) similar to that of the

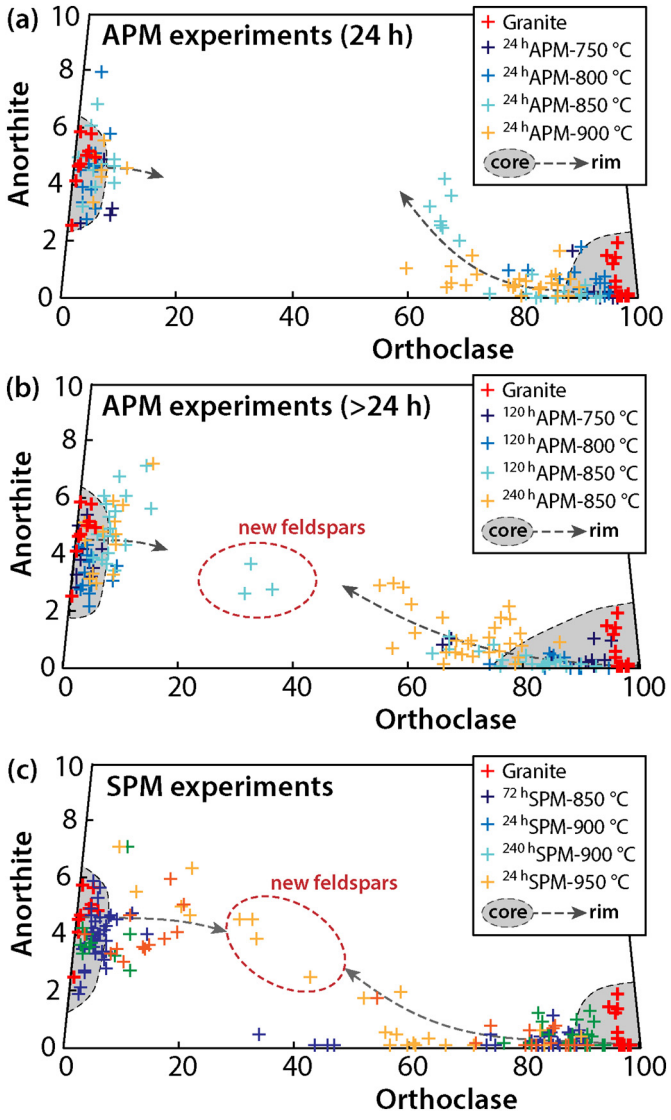

Fig. 9. Composition of feldspars analysed in (a-b) APM and (c) SPM experiments in a section of a ternary diagram Anorthite-Orthoclase-Albite (missing). Experiments with run durations of less (a) and >24 h (b) are reported separately for clarity. Compositions of feldspars analysed in the granite are shown for comparison (red crosses). Grey arrows indicate core-to-rim compositional variations.

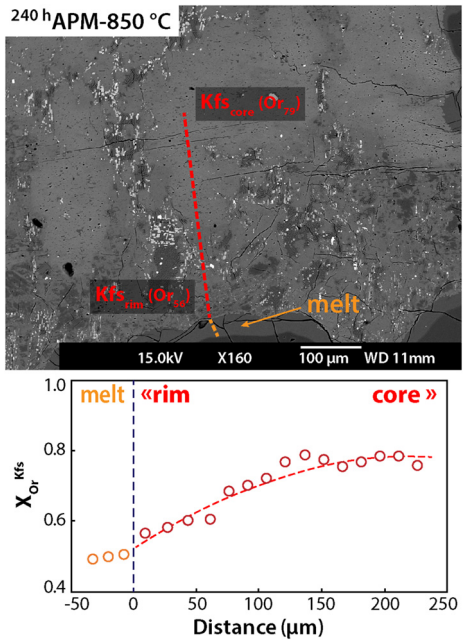

Fig. 10. (a) BSE image of a K-feldspar from the APM experiment run at 850 °C for 240 h and (b) compositional core-to-rim profile (X_{Or}) determined using EMP.

recrystallized feldspar rims (Table EA2). Variations in the compositions of feldspars are more evident along core-to-rim transverses, where smooth profiles are observed: an example of a compositional transverse of a K-feldspar from the 240 h experiment at 850 °C is shown in Fig. 10. The profile clearly shows a smooth change of composition from $Ab_{20}Or_{80}$ at the core to $Ab_{40}Or_{56}$ at the rim (An never exceeds 3 wt%). It is important to note that neither the core nor the rim preserved the initial composition of the K-feldspar (before partial melting) and that the core displays a rather homogeneous composition ($Ab_{20–24}Or_{73–79}$).

Feldspars analysed in SPM experiments exhibit smaller compositional variations compared to those in APM experiments (Fig. 9c), limited to the minerals in contact with either the haplogranitic melt channel or with the intergranular melt produced during partial melting. Similar to APM experiments, albite and K-feldspars are enriched in the Or and Ab components, respectively (Table EA2), and exhibit core-to-rim variations, whereas the newly formed feldspars have ternary sodic compositions ($An_{0-5}Ab_{40-70}Or_{27–58}$).

4. Discussion

4.1. Mechanisms of partial melting

The variability of texture and mineral assemblage observed in this study is the result of two main mechanisms of partial melting operating separately or conjointly: (1) dehydration melting (*i.e.* breakdown) of muscovite and (2) melting at grain boundaries. The first reaction depends solely on the local mineral assemblage whereas the second is regulated by the texture of mineral grains and depends on the general equilibrium minimum melting (Patiño-Douce, 1999). In the granite used in our experiments, muscovite breakdown and (subsolidus) formation of corundum initiates at 750 °C, whereas melting occurs pervasively at the quartz-feldspar grain boundaries and in fractures within quartz only at temperatures above 800 °C, assisted by the water released during the breakdown of muscovite. The two mechanisms are more effective with increasing time, temperature and water content. At 800 °C and anhydrous conditions, muscovite breakdown is still incomplete even in the long duration run (120 h). At 850 °C muscovite is completely dissolved and replaced by large patches of melt, K-feldspar and corundum (Fig. 3c–d). Upon complete muscovite breakdown, the melt fraction increases from 5 to 10 vol%, resulting in a decrease of melt water content from 7 to 8 wt% to 4–6 wt% (experiments at 500 MPa; Fig. 6b). Under hydrous conditions, complete muscovite breakdown is observed already at 800 °C and the amount of partial melting is twice that of the anhydrous experiment at 850 °C, suggesting that the influence of muscovite breakdown on melting at the grain boundaries is of secondary importance compared to partial melting assisted by fluids. Although no hydrous experiments were performed below 800 °C, we hypothesize that the presence of water would probably shift the breakdown reaction to temperatures as low as 750 °C. A similar result was obtained by Brearley and Rubie (1990), who pinpointed the breakdown of muscovite + quartz mineral assemblage in the presence of water at 757 °C, obtaining a texture similar to that of our APM experiments at 800 and 850 °C. In addition to biotite and K-feldspar, the experiments of Brearley and Rubie (1990) produced mullite ($Al_6Si_2O_{13}$), which is absent from our partial melting experiments because of the co-saturation of corundum and K-feldspar.

Our experimental observations are consistent with muscovite breakdown reactions occurring in the quartz-saturated KASH system, producing K-feldspar and aluminosilicate according to the reaction (Spear, 1993; Spear et al., 1999):

$$\text{Muscovite} + \text{Quartz} \rightarrow \text{Aluminosilicate} + \text{K}-\text{feldspar} + \text{melt} \quad (1)$$

The crystallization of corundum (Al_2O_3), rather than aluminosilicate (Al_2SiO_5), and biotite is due to the supersaturation of alumina (ASI > 1) and the water in the melt consequent to the rapid dissolution of muscovite. Patches of corundum, K-feldspar and biotite are in fact observed in the HPM experiment at 800 °C (Fig. 3g), despite the relatively high degree of partial melting (25–30 vol% melt; Table 1). At degrees of partial melting higher than 30%, the increasing melting of the quartz + feldspar mineral assemblage (muscovite is already dissolved) decreases the ASI of the melt to a value of about 1 and corundum is no longer present (Table EA1).

In contrast to the melt pockets produced during the breakdown of muscovite, no crystallization occurred in the melt layers formed during melting at the grain boundaries. The average thickness of these layers increases as partial melting progresses, up to values of about 30%. At higher values, melting occurs pervasively within feldspars (preferentially oriented along cleavage planes), producing sieve textures in relic feldpsars and leaving space for large pockets of melt around relic quartz crystals (Fig. 3h). The textural evolution during partial melting is controlled by the size and distribution of mineral grains, determining the number of triple junctions where melting initiates (eutectic melting) and the consequent melt percolation along mineral boundaries or within mineral fractures. The latter mechanism is indeed required to induce melting even at temperatures below two-minerals eutectics, through the transfer of eutectic chemical components (Mehnert et al., 1973).

4.2. Partial melting and melt composition

The interplay between dehydration melting and melting at the grain boundaries controls the evolution of melt composition at increasing degrees of partial melting. Indeed, the two mechanisms produced melts with different compositions that mixed in variable proportions. At relatively low degrees of partial melting (<10 vol% melt), the composition of the melt at the grain boundaries is similar to that of the bulk granite in terms of SiO_2 and total alkali (though with different FeO, CaO and Na_2O/K_2O ratio), whereas the melt in the pockets yields much lower SiO_2 concentrations and higher K_2O due to dissolution of muscovite (Fig. 6a; Table EA1). At increasing degrees of partial melting (10–20 vol% melt) and upon complete dissolution of muscovite, the melt produced by muscovite breakdown mixes with the more silicic melt produced at grain boundaries, and the overall melt composition becomes more homogeneous, though not exactly reproducing the composition of the bulk granite. The mixing of the two melt components is evident from the alignment of glass analyses along trends defined by the mineral phase undergoing melting (Fig. 6a). The evolution of the melt composition is consistent with previous experimental work (Mehnert et al., 1973; Watson and Jurewicz, 1984; Devineau et al., 2005) and confirms the systematic behaviour of the kinetics of melting for natural mineral aggregates (Acosta-Vigil et al., 2006). At increasingly higher degrees of partial melting (>20 vol% melt; HPM experiments), the changing mineral proportions determine an abrupt change of melt composition. The presence of relic quartz in the experiment at 900 °C indicates that non-modal melting occurs until all other minerals are consumed, thus explaining the unexpected depletion of the melt in SiO_2 at degrees of partial melting increasing from 20 to 70 vol% (Fig. 6a). Further melting of the relic quartz crystals would in fact move the composition of the melt towards the bulk composition of the granite.

Glass compositions of SPM experiments plot along a negative trend in a SiO_2*vs.* total alkali diagram, with the bulk composition of the synthetic haplogranite lying in the middle of this trend (Fig. 6c). In particular, the composition of the haplogranite glass is shifted either towards compositions less enriched in SiO_2 (24 h experiments at 850 and 900 °C) or towards compositions more enriched in SiO_2 (240 h experiment at 900 °C and 24 h experiment at 950 °C). The shift in composition depends on the composition and amount of the melt produced during partial melting and eventually mixed with the haplogranite. This confirms that, although not evident from the texture of the granite, partial melting occurred in an amount comparable to that observed in APM and HPM experiments performed at a given temperature. The depletion or enrichment in SiO_2 is thus related to the variable contribution of dehydration melting and melting at the grain boundaries prevailing at lower (melt < 10 vol%) and higher (melt = 10–20 vol%) degrees of partial melting, respectively. In parallel, the increasing partial melting produces a depletion in Na_2O and an increase of the ASI value that is consistent with the mixing between the haplogranite and a melt having a composition more similar to that of the bulk granite (Fig. 6d).

The extensive crystallization of the hydrous trachyandesite in ASM experiments increased the concentration of water in the melt phase, causing the complete melting of the granite at all experimental temperatures. This result was somehow unexpected, as relic quartz grains were present in the HPM experiment at 900 °C. The faster dissolution kinetics observed in ASM experiments can be thus explained by a more efficient melting at the grain boundaries, in the presence of a H_2O-saturated melt carrying the chemical components of missing eutectic phases (Mehnert et al., 1973). Relevant to this point, it is worth mentioning the primary effect of hydrous melts in reducing the timescale of assimilation, as deduced from short duration (*i.e.* minutes) experiments of carbonate assimilation by a hydrous andesitic melt (Blythe et al., 2015). In our experiments, the flux of H_2O and other chemical components from the trachyandesitic towards the granitic melt was regulated by both chemical diffusion and migration of a fluid phase exsolved from the crystal-rich trachyandesite. The combination of the two mechanisms overall produced a rather homogeneous concentration of dissolved H_2O at the length scale of the capsule already at 24 h and the formation of a hybrid trachytic melt at 240 h (Fig. 8). The thick layer of bubbles along the contact with the molten granite (Fig. 5d), however, suggests that migration of the exsolved fluid phase was the most efficient mechanism in hydrating the granitic melt. The fast kinetics of volatile transfer are consistent with experiments by Pistone et al. (2017), who also observed a rapid (<24 h) migration of H_2O from a hydrous trachyandesite to an anhydrous dacite. Besides favouring the rapid assimilation of the granite, the flux of H_2O from the crystallizing trachyandesite decreased the viscosity of the granitic melt and favoured the chemical homogenization (as observed from the chemical profile derived at 240 h; Fig. 8b). This is in apparent contradiction to the common assumption that melt homogenization is caused by convective stirring (*e.g.* in silicic magma chambers; Lindsay et al., 2001; Christiansen, 2005). Instead, we speculate that, at the scale of the experiment, chemical homogenization was simply driven by chemical diffusion, since sodium is able to diffuse over several millimetres during the longest experiments (Na diffusivity ~ 4.10^{-11} m^2/s in rhyolite; Henderson et al., 1985). Another remarkable point is the rapid time-scale of segregation of interstitial melt formed within the trachyandesite domains and of its mixing with the granitic melt, producing a nearly homogeneous composition intermediate between the bulk granite and trachyandesite (Fig. 8a). The crystal layers at the interface between the two domains act as a selective barrier, allowing only the transfer of melt and H_2O. The absence of mingling results in a lack of deformation features: to mingle, crystal-rich magmas (>50 vol%) have to deform together, which occurs only under specific rheological conditions (low viscosity contrast between end-members, for instance; Laumonier et al., 2014a). However, mixing textures may still develop even without deformation in dry or hydrous magmas (Laumonier et al., 2014b, 2015). Therefore, the few patches of clinopyroxene crystals embedded in the felsic molten component cannot be mingling features between the trachyandesite and the granite

(Fig. 5). We interpret these clinopyroxene patches to be the result of local heterogeneities from the granite, or gravitational movements like sinking parcels of trachyandesite or blobs segregated by rising bubbles (Wiesmaier et al., 2015). The large size of those clinopyroxene grains (up to 80 μm) and the skeletal shape compared to clinopyroxene from the trachyandesitic magma suggests that they grew relatively fast in the felsic host, likely doped by chemical components originating from the felsic magma.

4.3. Timescale for mineral-melt re-equilibration

At the conditions investigated by our experiments, re-equilibration between mineral and melt becomes effective within days. At anhydrous conditions and run durations of 120–240 h, feldspars that underwent re-equilibration with the melt exhibit distinct compositional trends with increasing Ab (K-feldspar) or Or (albite) components towards the rims (Figs. 9b). In particular, the An-Ab exchange constant (K_D $(An\text{-}Ab)^{pl\text{-}liq}$) of the albitic feldspar (240 h experiment at 850 °C; Fig. 10) decreases from 0.42 at the core to 0.09 at the rim, approaching the equilibrium value of 0.10 ± 0.05 expected at $T < 1050$ °C (Putirka, 2005, 2008). Similarly, the values of the Or-Ab exchange constant (K_D $(Or\text{-}Ab)^{pl\text{-}liq}$) calculated for all feldspar-melt pairs are very close to the equilibrium values predicted by the model of Mollo et al. (2015). The presence of water in the system undoubtedly enhances the chemical and textural re-equilibration of minerals, inducing the dissolution and re-crystallization of the original feldspars and crystallization of new ones. All the newly formed feldspars exhibit ternary sodic composition and euhedral morphology (Fig. 3e, g; Fig. 9b, c). Consistent with our results, partial melting experiments of a leucogranite by Acosta-Vigil et al. (2006), performed at P_{H2O} of 200 MPa and at temperatures between 690 and 800 °C, demonstrate mineral breakdown and crystallization of new feldspars in a relatively short time (generally within 24 h). However, equilibration between partial melt and residual minerals in the leucogranite required much longer times than in the granite used in this study: the melts produced by Acosta-Vigil et al. (2006) in experiments performed at 800 °C and with durations of >7 days show quite heterogeneous composition, whereas, in contrast, the melt produced in all HPM experiments is rather homogeneous after 24 h (SiO_2 and alkalis vary within 3 wt% and 1.5 wt%, respectively; Table EA1). These observations led the authors to conclude that both the near-minimum composition of (disequilibrium) partial melt and the composition of residual feldspars may persist for up to at least three months. In contrast, early re-equilibration was observed in partial melting experiments of a felsite from Krafla volcano (Iceland) from Masotta et al. (2018), where compositional changes of melt and minerals occurred after relatively short run durations (48 h). Such different evolutions towards equilibrium between melt and mineral indicate that equilibration kinetics strongly depend on the chemical composition of the system and the mineral phases considered. In fact, it is worth noting that equilibration of plagioclase is extremely slow compared to that of K-feldspar (Johannes, 1978, 1989; Johannes and Holtz, 1992), which may explain the relatively fast re-equilibration of alkali feldspars compared to the anorthitic feldspar obtained by Acosta-Vigil et al. (2006).

4.4. Melt segregation and trace element transport

Melt veins formed at the grain boundaries within the granite regions of the SPM experiments are significantly thinner (generally <5 μm or even absent for run durations lower than 72 h) compared to those produced in APM experiments performed at the same conditions. Possibly, this feature results from local pressure gradients, due to a different response to the pressure of the grain matrix with respect to the melt region: newly formed melt is expelled out of the granite and segregates in the central haplogranite channel. This hypothesis is supported by the change in composition of the haplogranitic melt (Fig. 6c–d; see Section 5.2) and the lack of distinct core-to-rim compositional variation of feldspars within the granite regions (compared to those observed in APM experiments; Fig. 10). The latter feature denotes a rapid time scale for melt production and segregation that prevented any exchange between the melt and the feldspars. Indeed, remarkable compositional variations are observed only in feldspars in contact with the haplogranitic melt channel and those that underwent dissolution and re-crystallization (Fig. 9c).

Another possible mechanism generating pressure gradients and explaining the segregation of the melt produced at grain boundaries within the central haplogranite channel could be the change in volume during melting of the two domains. The volume of granite undergoing partial melting is expected to increase ($\Delta V > 0$), whereas melting of the haplogranitic glass powder in the central channel would result in a volume decrease due to compaction and pore reduction during melting (this is deduced from the inward inflection of the capsule lid in some experiments; Fig. 4b). A similar trade-off in the volume change is expected to occur in igneous complexes when granitic rocks undergoing partial melting are cross-cut by silicic melt veins, such as aplites.

As a result of the compaction-melt extraction process, the melt pockets produced by the breakdown of muscovite are much smaller than those observed in APM and HPM experiments. Given the lower fraction of interstitial melt, early water saturation occurred by muscovite breakdown. Bubbles are indeed observed in the melt veins connecting the melt pockets with the haplogranitic channel and within the haplogranite adjacent to these veins, where small bubbles probably coalesced into larger ones that did not have enough time to further dissolve in the haplogranite (Fig. 4b). The presence of these bubbles provides further evidence of melt and water transport from the granite to the central melt channel, and indicates that permeability is achieved even at very low degrees of partial melting, such as demonstrated experimentally in a partially molten olivine aggregate with low melt fractions (<0.5%; Laumonier et al., 2017).

Based on our experiments, we confirm the strong link between the degree of partial melting and the evolution of the melt composition produced by transfer of volatiles and incompatible trace elements. For instance, the lowest degree of partial melting (72 h experiment at 850 °C and 24 h experiment at 900 °C) produced the highest enrichment of Li and Sr but the lowest enrichment of Cs and Pb (Fig. 7b). Li and Sr are more compatible in feldspars than in other mineral phases and their early enrichment indicates: (i) prevailing feldspar dissolution at an early stage of partial melting and (ii) fast diffusion within the haplogranite. The upward curved profiles of Li and Sr are in fact due to the higher diffusivity of these elements (ranging from 10^{-9} to 10^{-12} m^2/s; Jambon and Semet, 1978; Behrens and Hahn, 2009) with respect to Pb and Cs (ranging from 10^{-13} to 10^{-15} m^2/s; Jambon, 1982; Roselieb and Jambon, 1997), whose profile rather indicates their concentration at the interface between the granite and the haplogranitic melt. In contrast to Li and Sr, the enrichment in Pb and Cs is higher in the experiment with the highest degree of partial melting (240 h experiment at 900 °C), indicating that these two elements are released in equal proportions from mineral phases undergoing dissolution. Indeed, in this experiment, the concentration of Pb and Cs is maximum in secondary veins formed after the disruption of the granite, where interstitial melt accumulated after segregation from the granite (spot analyses #5 and #10 in Fig. 4c; Table EA3). In the same points, consistently, crystallization of feldspar produced a depletion of both Li and Sr (Fig. 7b). The peculiar distribution of these trace elements accounts for an initial homogeneous cation distribution within the dissolving minerals, which is consistent with the rather homogeneous composition of feldspars in the starting granite (Fig. 9).

4.5. Implications for natural systems

Although magmatic differentiation is likely the most efficient mechanism in subduction areas (Annen et al., 2005), *in situ* partial melting

could dominate the crustal differentiation in orogenic convergent settings (*e.g.*Bergantz, 1989; Vielzeuf and Holloway, 1988). The results from the three experimental setups consistently indicate that granitic melt can rapidly form by dehydration melting of hydrous minerals or at feldspar-quartz boundaries and easily segregate into silicic dikes and veins. Silicic segregations induced by partial melting of granitic rocks have been commonly observed in natural systems (Hersum et al., 2007; Petcovic and Grunder, 2003; Philpotts and Asher, 1993), yet the mechanisms of melt segregation are quite complex and depend on the interplay between volume changes during rock-melt interaction and the grain-scale to regional stress regime. Rocks undergoing partial melting are likely to expand, promoting the formation of fractures in the host where the melt could escape. Partial melting is, indeed, frequently observed as melt-filled intra-crystalline micro-cracks (Holness and Watt, 2002). On the other hand, contraction during magma solidification and relaxation of overpressure during fracture opening increases the differential stress that favors the compaction of the rock undergoing partial melting, improving melt segregation (Hersum et al., 2007). In other words, segregation is likely to become self-sustaining once partial melting has started and new fractures are created, so that the melt produced accumulates either on top of the intrusive body as a sill or into newly opened fractures. An example of this situation could be the rhyolitic sill intercepted during perforation IDDP-1 at the Krafla caldera (Iceland), a meters-thick sill of liquid magma emplaced within a partially molten felsite (Zierenberg et al., 2013).

Melts produced by partial melting of granitic rocks display enrichment in incompatible trace elements, in amounts that are inversely proportional to the degree of partial melting (Hanson, 1978). Trace element profiles along and across the haplogranitic channel of SPM experiments result from: (1) element mobility that depends on both diffusivity and compatibility within the structure of minerals in contact with melt, (2) partial melting of the source granite and (3) segregation into the central haplogranitic channel. At open system conditions, likely corresponding to natural conditions, chemical diffusion is of secondary importance compared to mass transport controlled by melt and/or fluid flow within the channel. The presence of a fluid phase (H_2O, CO_2, salted solutions) undoubtedly enhances the mobility of some elements and may favour their transport to a greater distance from their source. A similar mechanism was proposed by Jahns and Burnham (1969) to explain the formation of pegmatites through buoyant separation of an aqueous fluid from a silicate melt. Despite the fact that the channel of haplogranite was artificially created, the configuration of SPM experiments can be viewed as reproducing the emplacement of a pegmatitic vein network. Pegmatites usually occur as segregations within granites or as discordant dikes intruding igneous and metamorphic complexes, and exhibit fabrics and mineral assemblages that distinguish from the more common and voluminous plutonic igneous rocks (London and Kontak, 2012). It is generally accepted that the peculiar texture observed in pegmatites results from undercooling crystallization of residual melts, highly enriched in fluid and incompatible components, fractionated after an extensive differentiation in an essentially closed system (London, 2008). Based on our experiments, we conclude that partial melting and segregation can transport melt with high volatile and incompatible trace element contents, thus representing a plausible mechanism to produce pegmatitic veins. Such a mechanism is an alternative to the typical late crystallization of a pluton associated with the release of fluids (London, 2008).

Preserved heterogeneous domains produced in ASM experiments mimic natural granitic complexes where the emplacement of mafic magmas at shallow depths results in the assimilation of the granitic host, thus producing hybrid lithologies. Natural examples of such a scenario can be found worldwide in complexes associated with mafic rocks and containing abundant mafic magmatic enclaves (see Didier and Barbarin, 1991 and references therein). Such enclaves often exhibit bulk compositional diversities that reflect the different stages of hybridization and digestion by the host granitites (Barbarin, 2005). The rheological contrast between both mafic and felsic domains determines the extent of the interaction. In the case of mafic and felsic domains exhibiting very different crystal contents (as in the case of the ASM experiments), the contrast in bulk viscosity is likely to prevent any interaction but rather favors the formation of heterogeneous parcels limited to the interface between the two end-members (Laumonier et al., 2014a). A natural equivalent of these heterogeneous domains is represented by crystal-rich rocks that show contrasting mineral assemblages with textural and chemical features that are often associated with crystal mush settings (Holness and Bunbury, 2006; Masotta et al., 2016; Tait et al., 1989). The differences in the physical state and mechanical behaviour of crystal-rich and crystal-poor domains in mush settings are responsible for a number of processes, including defrosting, remobilization and rejuvenation of crystal mushes as well as crystal-melt separation and volatile transfer (Bachmann and Bergantz, 2004; Burgisser and Bergantz, 2011; Huber et al., 2010; Masotta et al., 2012b; Parmigiani et al., 2016). By analogy with the experiment where the feldspar-rich layer represents a barrier through which melt and H_2O migrate at different rates, crystal-rich boundary layers in natural systems are likely to permit mass transfer from one domain to another, although preventing them from mingling. In particular, transfer of volatiles through migration of an exsolved phase (*e.g.*Pistone et al., 2017) may act on a very short time scale, allowing hydration melting of the assimilated host, favouring segregation of the interstitial melt and reducing overall the time scale for melt hybridization.

5. Conclusion

Three different experimental setups were used (with no pretention to achieve thermodynamic equilibrium) to reproduce conditions under which partial melting of granitic crust occurs in nature. The distribution and chemical composition of the melt produced at anhydrous conditions is essentially controlled by the abundance of hydrous minerals and, at increasing temperature, by the grain texture and mineral proportions. A very low amount of water in the system (<1 wt%) is sufficient to wet grain contacts, which lowers the temperature required to initiate partial melting at anhydrous conditions by about 100 °C. Melt produced at the grain boundaries can be rapidly segregated into silicic dikes and veins, if lateral pressure gradients exist at the local/regional scale or originate in response to system expansion and contraction during partial melting. Residual minerals may not record partial melting if they have insufficient time to re-equilibrate with the melt before melt segregation. In this case, the melt segregated into dikes and veins behaves like a vector for incompatible elements that are accumulated and transported, likely assisted by a fluid phase. Partial melting accompanied by fluid-assisted melt segregation thus represents a plausible mechanism for generation of pegmatites. Lastly, full melting of granitic rocks during the intrusion of a hydrous intermediate magma can generate batches of hybrid rhyolitic melts. The difference in crystallinity between the two magma domains may prevent the mingling of the two magmas, limiting their interaction to the flux of melt and volatiles between the two.

Acknowledgments

The present experimental work has been carried out mostly during the Short Course on “High-Pressure Experimental Techniques and Applications to the Earth's Interior” held at BGI in the years 2013, 2014 and 2015. Piston cylinder experiments were performed by the students who attended the Short Course under the supervision of BGI researchers Andreas Audédat, Catherine McCammon, Matteo Masotta and Svyatoslav Shcheka. Andreas Audédat also assisted during LA-ICP-MS analyses. We are grateful to H. Schulze for help with sample preparation and to D. Krauße for help with the microprobe analyses. Massimo D'Orazio is acknowledged for assistance with ICP-MS analyses. Mario Gaeta and Silvio Mollo are acknowledged for constructive reviews.

Appendix A. Supplementary data

Supplementary data to this article can be found online at https://doi.org/10.1016/j.lithos.2018.08.032.

References

Acosta-Vigil, A., London, D., Morgan VI, G.B., 2006. Experiments on the kinetics of partial melting of a leucogranite at 200 MPa H_2O and 690–800°C: compositional variability of melts during the onset of H_2O-saturated crustal anataxis. Contrib. Mineral. Petrol. 151, 539–557.

Al-Rawi, Y., Carmichael, I.S.E., 1967. Natural fusion of granite. Am. Mineral. 52, 1806–1814.

Annen, C., Blundy, J.D., Sparks, R.S.J., 2005. The genesis of intermediate and silicic magmas in deep crustal hot zones. J. Petrol. 47 (3), 505–539.

Attrill, P.G., Gibb, F.G.F., 2003a. Partial melting and recrystallization of granite and their application to deep disposal of radioactive waste part 1—Rationale and partial melting. Lithos 67, 103–117.

Attrill, P.G., Gibb, F.G.F., 2003b. Partial melting and recrystallization of granite and their application to deep disposal of radioactive waste part 2—Recrystallization. Lithos 67, 119–133.

Audédat, A., Pettke, T., 2006. Evolution of a porphyry-cu mineralized magma system at Santa Rita, New Mexico (USA). J. Petrol. 47, 2021–2046.

Bachmann, O., Bergantz, G.W., 2004. On the origin of crystal-poor rhyolites: extracted from batholithic crystal mushes. J. Petrol. 45, 1565–1582.

Barbarin, B., 2005. Mafic magmatic enclaves and mafic rocks associated with some granitoids of the Central Sierra Nevada batholith, California: nature, origin, and relations with the hosts. Lithos 80, 155–177.

Behrens, H., Hahn, M., 2009. Trace element diffusion and viscous flow in potassium-rich trachytic and phonolitic melts. Chem. Geol. 259, 63–77.

Bergantz, G.W., 1989. Underplating and partial melting: implications for melt generation and extraction. Science 245, 1093–1095.

Blythe, L.S., Deegan, F.M., Freda, C., Jolis, E.M., Masotta, M., Misiti, V., Taddeucci, J., Troll, V. R., 2015. CO_2 bubble generation and migration during magma–carbonate interaction. Contrib. Mineral. Petrol. 169, 42.

Brearley, A.J., Rubie, D.C., 1990. Effects of H_2O on the disequilibrium breakdown of Muscovite + Quartz. J. Petrol. 31, 925–956.

Burgisser, A., Bergantz, G.W., 2011. A rapid mechanism to remobilize and homogenize crystalline magma bodies. Nature 471, 212–215.

Christiansen, E.N., 2005. Contrasting processes in silicic magma chambers: evidence from very large volume ignimbrites. Geol. Mag. 142, 669–681.

Clemens, J.D., 1984. Water contents of intermediate to silicic magmas. Lithos 17, 273–287.

Clemens, J.D., Droop, G.T.R., 1998. Fluids, P–T paths and the fates of anatectic melts in the earth's crust. In: Clemens, J.D., Hutton, D.H. (Eds.), Generation of Granitic Rocks and Deep Crustal Processes. vol. 44. Lithos, pp. 21–36.

Clemens, J.D., Vielzeuf, D., 1987. Constraints on melting and magma production in the crust. Earth Planet. Sci. Lett. 86, 287–306.

Devine, J.D., Gardner, J.E., Brack, H.P., Layne, G.D., Rutherford, M.J., 1995. Comparison of microanalytical methods for estimating H_2O contents of silicic volcanic glasses. Am. Mineral. 80, 319–328.

Devineau, K., Pichavant, M., Villiéras, F., 2005. Melting kinetics of granite powder aggregates at 1175°C, 1 atm. Eur. J. Mineral. 17, 387–398.

Didier, J., Barbarin, B. (Eds.), 1991. Enclaves and Granite Petrology, Developments in Petrology. vol. 13. Elsevier, Amsterdam.

Fyfe, W.S., 1970. Some thoughts on granitic magmas. In: Newall, G., Rast, N. (Eds.), Mechanism of Igneous Intrusion. Geological Journal Special Issue. 2, pp. 201–216.

Gaeta, M., Giuliani, A., Perilla, S., Misiti, V., 2013. Reddish Metagranites from the Gennargentu Igneous complex (Sardinia, Italy): Insight into Metasomatism Induced by Magma Mingling. J. Petrol. 54, 839–859.

Gaeta, M., Giuliani, A., Di Rocco, T., Tecchiato, V., Perinelli, C., Kamenetsky, V.S., 2018. Isotopic disequilibrium in migmatitic hornfels of the Gennargentu Igneous complex (Sardinia, Italy) records the formation of low $^{87}Sr/^{86}Sr$ melts from a mica-rich source. J. Petrol. https://doi.org/10.1093/petrology/egy062 accepted.

Hanson, G.N., 1978. The application of trace elements to the petrogenesis of igneous rocks of granitic composition. Earth Planet. Sci. Lett. 38, 26–43.

Henderson, P., Nolan, J., Cunningham, G.C., Lowry, R.K., 1985. Structural controls and mechanisms of diffusion in natural silicate melts. Contrib. Mineral. Petrol. 89, 263–272.

Hersum, T.G., Marsh, B.D., Simon, A.C., 2007. Contact partial melting of granitic country rock, melt segregation, and re-injection as dikes into Ferrar Dolerite Sills, McMurdo Dry Valleys, Antarctica. J. Petrol. 48, 2125–2148.

Holness, M.B., Bunbury, J.M., 2006. Insights into continental rift-related magma chambers: Cognate nodules from the Kula Volcanic Province, Western Turkey. J. Volcanol. Geotherm. Res. 153, 241–261.

Holness, M.B., Watt, G.R., 2002. The aureole of the Traigh Bhàn na Sgùrra Sill, Isle of Mull: reaction-driven micro-cracking during pyrometamorphism. J. Petrol. 43, 511–534.

Holness, M.B., Dane, K., Sides, R., Richardson, C., Caddick, M., 2005. Melting and melt segregation in the aureole if the Glenmore Plug, Ardnamurchan. J. Metamor. Petrol. 23, 29–43.

Huber, C., Bachmann, O., Manga, M., 2010. Two competing effects of volatiles on heat transfer in crystal-rich magmas: thermal insulation vs defrosting. J. Petrol. 51, 847–867.

Jahns, R.H., Burnham, C.W., 1969. Experimental studies of pegmatite genesis: I. A model for the derivation and crystallization of granitic pegmatites. Econ. Geol. 64, 843–864.

Jambon, A., 1982. Tracer diffusion in granitic melts: experimental results for Na, Rb, Cs, Ca, Sr, Ba, Ce, Eu to 1300 °C and a model of calculation. J. Geophys. Res. 87, 10797–10810.

Jambon, A., Semet, M.P., 1978. Lithium diffusion in silicate glasses of albite, orthoclase, and obsidian compositions: an ion-microprobe determination. Earth Planet. Sci. Lett. 37, 445–450.

Johannes, W., 1978. Melting of plagioclase in the system Ab–An–H_2O and Qz–Ab–An–H2O at PH_2O=5 kbar, an equilibrium problem. Contrib. Mineral. Petrol. 66, 295–303.

Johannes, W., 1989. Melting of plagioclase–quartz assemblages at 2 kbar water pressure. Contrib. Mineral. Petrol. 103, 270–276.

Johannes, W., Holtz, F., 1992. Melting of plagioclase in granite and related systems: composition of coexisting phases and kinetic observations. Trans. Royal Soc. Edinburgh 83, 417–422.

Johannes, W., Holtz, F., 1996. Petrogenesis and Experimental Petrology of Granitic Rocks. Springer-Verlag, New York.

Kaczor, S.M., 1988. Disequilibrium melting of granite at the contact with a basic plug: a geochemical and petrographic study. J. Geol. 96, 61–78.

Kriegsman, L.M., 2001. Partial melting, partial melt extraction and partial back reaction in anatectic migmatites. Lithos 56, 75–96.

Laumonier, M., Scaillet, B., Pichavant, M., Champallier, R., Andujar, J., Arbaret, L., 2014a. On the conditions of magma mixing and its bearing on andesite production in the crust. Nat. Commun. 5, 5607.

Laumonier, M., Scaillet, B., Arbaret, L., Champallier, R., 2014b. Experimental simulation of magma mixing at high pressure. Lithos 196, 281–300.

Laumonier, M., Scaillet, B., Arbaret, L., Andújar, J., Champallier, R., 2015. Experimental mixing of hydrous magmas. Chem. Geol. 418, 158–170.

Laumonier, M., Farla, R., Frost, D.J., Katsura, T., Marquardt, K., Bouvier, A.S., Baumgartner, L. P., 2017. Experimental determination of melt interconnectivity and electrical conductivity in the upper mantle. Earth Planet. Sci. Lett. 463, 286–297.

Le Breton, N., Thompson, A.B., 1988. Fluid-absent dehydration. Melting of biotite in metapelites in the early stages of crustal anatexis. Contrib. Mineral. Petrol. 99, 226–237.

Lindsay, J.M., Schmitt, A.K., Trumbull, R.B., de Silva, S.L., Emmermann, R., 2001. Magmatic evolution of the La Pacana caldera system, Central Andes, Chile: compositional variation of the two cogenetic, large-volume felsic ignimbrites. J. Petrol. 42, 459–486.

London, D., 2008. Pegmatites. Can. Mineral. Special Publ. 10 (368 pp.).

London, D., Kontak, D.J., 2012. Granitic Pegmatites: Scientific Wonders and Economic Bonanzas. Elements 8, 257–261.

London, D., Morgan VI, G., 2012. The pegmatite puzzle. Elements 8, 263–268.

Luth, W.C., 1969. The systems $NaAlSi_3O_8$–SiO_2 and $KAlSi_3O_8$–SiO_2 to 20 kb and the relationship between H_2O-content, P_{H2O}, and P_{total} in granitic magmas. Am. J. Sci. 267, 325–341.

Masotta, M., Keppler, H., 2015. Anhydrite solubility in differentiated arc magmas. Geochim. Cosmochim. Acta 185, 79–102.

Masotta, M., Freda, C., Paul, T.A., Moore, G.M., Gaeta, M., Scarlato, P., Troll, V.R., 2012a. Low pressure experiments in piston cylinder apparatus: calibration of newly designed 25 mm furnace assemblies to P = 150 MPa. Chem. Geol. 312–313, 74–79.

Masotta, M., Freda, C., Gaeta, M., 2012b. Origin of crystal-poor, differentiated magmas: insights from thermal gradient experiments. Contrib. Mineral. Petrol. 163, 49–65.

Masotta, M., Mollo, S., Gaeta, M., Freda, C., 2016. Melt extraction in mush zones: the case of crystal-rich enclaves at the Sabatini Volcanic District (Central Italy). Lithos 248–251, 288–292.

Masotta, M., Mollo, S., Nazzari, M., Tecchiato, V., Scarlato, P., Papale, P., Bachmann, O., 2018. Crystallization and partial melting of rhyolite and felsite rocks at Krafla volcano: a comparative approach based on mineral and glass chemistry of natural and experimental products. Chem. Geol. 483, 603–618.

Mehnert, K.R., Büsch, W., Schneider, G., 1973. Initial melting at grain boundaries of quartz and feldspar in gneisses and granulites. Neues Jahrbuch für Mineralogie 4, 165–183.

Mollo, M., Masotta, M., Forni, F., Bachmann, O., De Astis, G., Moore, G., Scarlato, P., 2015. A K-feldspar–liquid hygrometer specific to alkaline differentiated magmas. Chem. Geol. 392, 1–8.

Parmigiani, A., Faroughi, S., Huber, C., Bachmann, O., Su, Y., 2016. Bubble accumulation and its role in the evolution of magma reservoirs in the upper crust. Nature 532, 492–495.

Patiño-Douce, A.E., 1999. What do experiments tell us about the relative contributions of crust and mantle to the origin of granitic magmas? In: Castro, A., Fernandez, C., Vigneresse, J.L. (Eds.), Understanding Granites. Integrating New and Classical Techniques. 158. Geological Society, London, pp. 55–75 Special Publications

Patiño-Douce, A.E., Beard, J.S., 1995. Dehydration-melting of biotite gneiss and quartz amphibolite from 3 to 15 kbar. J. Petrol. 36, 707–738.

Petcovic, H.L., Grunder, A.L., 2003. Textural and thermal history of partial melting in tonalitic wallrock at the margin of a basalt dike, Wallowa Mountains, Oregon. J. Petrol. 44, 2287–2312.

Pettke, T., Halter, W.E., Webster, J.D., Aigner-Torres, M., Heinrich, C.A., 2004. Accurate quantification of melt inclusion chemistry by LA-ICP-MS: a comparison with EMP and SIMS and advantages and possible limitations of these methods. Lithos 78, 333–361.

Philpotts, A.R., Asher, P.M., 1993. Wallrock melting and reaction effects along the Higganum diabase dike in Connecticut: contamination of a continental flood basalt feeder. J. Petrol. 34, 1029–1058.

Pistone, M., Blundy, J., Brooker, R.A., EIMF, 2017. Water transfer during magma mixing events: Insights into crystal mush rejuvenation and melt extraction processes. Am. Mineral. 102, 766–776.

Putirka, K., 2005. Igneous thermometers and barometers based on plagioclase + liquid equilibria: tests of some existing models and new calibrations. Am. Mineral. 90, 336–346.

Putirka, K., 2008. Thermometers and barometers for volcanic systems. Rev. Mineral. Geochem. 69, 61–120.

Qian, Q., Hermann, J., 2013. Partial melting of lower crust at 10–15 kbar: constraints on adakite and TTG formation. Contrib. Mineral. Petrol. 165, 1195–1224.
Roselieb, K., Jambon, A., 1997. Tracer diffusion of patassium, rubidium, and cesium in a supercooled jadeite melt. Geochim. Cosmochim. Acta 61, 3101–3110.
Scaillet, B., Pichavant, M., Roux, J., 1995. Experimental crystallization of leucogranite magmas. J. Petrol. 36, 663–705.
Spear, F.S., 1993. Metamorphic Phase Equilibria and Pressure– Temperature–Time Paths. Mineralogical Society of America, Washington, DC.
Spear, F.S., Kohn, M.L., Cheney, J.T., 1999. P-T paths from anatectic pelites. Contrib. Mineral. Petrol. 134, 17–32.
Stevens, G., Clemens, J.D., 1993. Fluid absent melting and the roles of fluids in the lithosphere: a slanted summary? Chem. Geol. 108, 1–17.
Tait, S.R., Wörner, G., Van Den Bogaard, P., Schminke, H.-U., 1989. Cumulate nodules as evidence for convective fractionation in a phonolite magma chamber. J. Volcanol. Geotherm. Res. 37, 21–37.
Thompson, A.B., 1982. Dehydration melting of pelitic rocks and the generation of H_2O-undersaturated granitic liquids. Am. J. Sci. 282, 1567–1595.
Tuttle, O.F., Bowen, N.L., 1958. Origin of granite in the light of experimental studies in the system $NaAlSi_3O_8$-$KAlSi_3O_8$-SiO_2-H_2O. Geol. Soc. Am. Bull. 104, 1–153.
Vielzeuf, D., Holloway, J.R., 1988. Experimental determination of the fluid-absent melting relations in the pelitic system. Contrib. Mineral. Petrol. 98, 257–276.
Watson, E.B., Jurewicz, S.R., 1984. Behavior of alkalies during diffusive interaction of granitic xenoliths with basaltic magma. J. Geol. 92, 121–131.
Weinberg, R.F., Hasalová, P., 2015. Water-fluxed melting of the continental crust: a review. Lithos 212–215, 158–188.
Wiesmaier, S., Morgavi, D., Renggli, C.J., Perugini, D., De Campos, C.P., Hess, K.U., Ertel-Ingrisch, W., Lavallée, Y., Dingwell, D.B., 2015. Magma mixing enhanced by bubble segregation. Solid Earth 6 (3), 1007.
Wolf, M.B., Wyllie, P.J., 1995. Liquid segregation parameters from amphibolite dehydration melting experiments. J. Geophys. Res. 100, 15611–15622.
Zierenberg, R.A., Schiffman, P., Barfod, G.H., Lesher, C.E., Marks, N., Lowenstein, J.B., Mortensen, A.K., Pope, E.C., Bird, D.K., Reed, M.H., Friðleifsson, G.Ó., Elders, W.A., 2013. Composition and origin of rhyolite melt intersected by drilling in the Krafla geothermal field, Iceland. Contrib. Mineral. Petrol. 165, 327–347.